2 Overview of the Research Field

2.1. Carbon & Carbon Nanotubes

2.1.1. Carbon Hybridization

Carbon is the main building block of the so-called Organic Chemistry, which comprehends a significant part of Chemistry. The existence of a whole area in Chemistry devoted to Carbon based substances owes to its element's flexibility in making chemical bonds, so that it is present in a myriad of compounds.

Carbon is the first element from the IV A family of the periodic table, and has the electronic configuration $1s^2 2s^2 2p^2$. This electronic structure causes the "chemical flexibility" the element, as will be described in the next paragraphs.

The $1s$ orbital composes a stable electronic configuration similar to Helium atom. The electrons present in this orbital are called core electrons, because they are the innermost electrons and are tightly bonded to the atom nucleus. These electrons do not participate in the chemical reactions of Carbon.

On the other hand, $2s$ and $2p$ orbitals participate on chemical reactions, because their binding energies are smaller, what makes their mixing easier. The mixing between orbitals of an atom in order to perform a chemical bonding is called hybridization. The ease of Carbon orbitals to hybridize is what makes this element prone to participate in a variety of different chemical bonds, and be present in a myriad of chemical species.

From an energetic point of view, when an atom approaches a Carbon atom, off-diagonal elements appear in the Hamiltonian owing to the perturbation caused by the neighboring atom. So, Carbon's original orbitals will mix in order to form an eigenfunction basis of the new Hamiltonian.

From a geometric standpoint, hybridization will happen in such a way that the new orbitals are biased in the direction of the neighboring atom.

Carbon atoms exist in chemical species under three main hybridizations of its $2s$ and $2p$ orbitals, which are called sp, sp^2, and sp^3.

2.1.1.1. sp Hybridization:

sp Hybridization corresponds to mixing $2s$ orbital with one of the $2p$ orbitals.

$$|sp_a> = C_1 \cdot |2s> + C_2 \cdot |2p_x>$$
$$|sp_b> = C_3 \cdot |2s> + C_4 \cdot |2p_x>$$

Equation (1)

PUC-Rio - Certificação Digital Nº 1011917/CB

The coefficients are obtained from orthonormality relationships, and from the knowledge of the molecule potential, or from symmetry considerations. In this case, requiring that the orbitals sp_a and sp_b be spatially symmetric in relation to one another yields the solution:

$$|sp_a> = \frac{1}{\sqrt{2}} \cdot (|2s> + |2p_x>)$$
$$|sp_b> = \frac{1}{\sqrt{2}} \cdot (|2s> - |2p_x>) \qquad \text{Equation (2)}$$

In fact, Figure 1 shows that the sp orbital of an C atom is prone to forming a strong bond with the neighboring atom's orbital; this bond is known as σ bond. The other $2p$ orbitals (in this case, $2p_y$ and $2p_z$), perpendicular to the sp orbitals, remain responsible for two weak bonds, which is called π bond, with the neighboring atom.

This hybridization is responsible for linear structures.

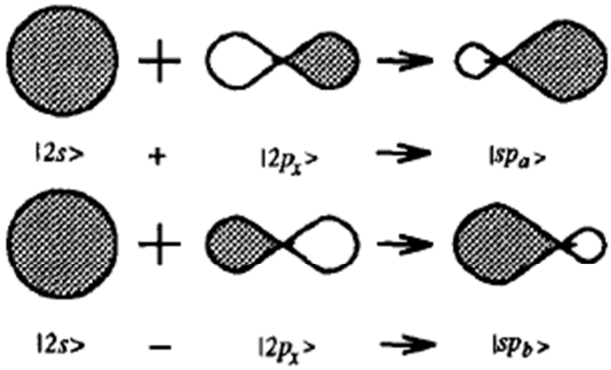

Figure 1: This picture, adapted from [2], shows the geometric character of sp hybridization: the symmetrical, and atom centered, $2s$ and $2p$ orbitals mix in order to create an orbital biased towards the neighboring atom, which attracts the electrons.

2.1.1.2. sp^2 Hybridization:

In this case, the $2s$ orbital mix with two $2p$ orbitals. This hybridization is related to trigonal planar structures, for example graphite.

When hybridizing $2p$ orbitals with each other, the result is only a rotation of the original $2p$ orbitals. The hybridization of an $2p$ orbital with an $2s$ orbital serves only to give the asymmetric shape, biased towards the neighboring atom.

As a consequence, in order to understand sp^2 hybridization, one must follow two steps. First, the two $2p$ orbitals are mixed in order to make three wavefunctions, with $120°$ angle between their directions. Then, the $2s$ orbitals are added to each wavefunction, taking into account orthonormality relations, in order to give the biasing character towards the neighboring atoms. The result is the following mathematical expressions:

PUC-Rio - Certificação Digital Nº 1011917/CB

$$|sp_a{}^2> = \frac{1}{\sqrt{3}} \cdot |2s> - \sqrt{\frac{2}{3}} \cdot |2p_y>$$

$$|sp_b{}^2> = \frac{1}{\sqrt{3}} \cdot |2s> + \sqrt{\frac{2}{3}} \cdot \left(\frac{\sqrt{3}}{2}|2p_x> + \frac{1}{2}|2p_y>\right) \quad \text{Equation (3)}$$

$$|sp_c{}^2> = \frac{1}{\sqrt{3}} \cdot |2s> + \sqrt{\frac{2}{3}} \cdot \left(-\frac{\sqrt{3}}{2}\left|2p_x> + \frac{1}{2}\right| 2p_y>\right)$$

The sp^2 orbitals make the σ bonds with the neighboring atoms, while the perpendicular $2p_z$ orbital makes the weaker π bond simultaneously with the three atoms.

sp^2 Hybridization is present in graphite, and graphene, where one can observe an hexagonal lattice composed of Carbon atoms, making with each other $120°$ bonds. It is approximately present in Carbon Nanotubes, since curvature of the walls of the tube imposes a bending of the orbitals off the sp^2 plane.

2.1.1.3. sp^3 Hybridization

In this hybridization all orbitals are mixed in order to create a tetrahedral volumetric structure.

In the same fashion as in the sp^2 case, first one mixes the three $2p$ orbitals in order to obtain the tetreahedral geometry, and then adds the $2s$ orbital, respecting orthonormality. The hybridized orbtials are given below:

$$|sp_a{}^3> = \frac{1}{2} \cdot (|2s> + |2p_x> + |2p_y> + |2p_z>)$$
$$|sp_b{}^3> = \frac{1}{2} \cdot (|2s> - |2p_x> - |2p_y> + |2p_z>)$$
$$|sp_c{}^3> = \frac{1}{2} \cdot (|2s> - |2p_x> + |2p_y> - |2p_z>) \quad \text{Equation (4)}$$
$$|sp_d{}^3> = \frac{1}{2} \cdot (|2s> + |2p_x> - |2p_y> - |2p_z>)$$

This hybridization is present in diamond, for example.

2.1.2. Carbon allotropes

Owing to the C atom capability of hybridizing its valence orbitals in a flexible way, this element can be found in nature in many different molecules. Chemistry has a whole area only to study molecules made of Carbons, which is organic chemistry.

Nonetheless, elemental Carbon exists in nature in basically two different structures: diamond and graphite. Both these materials are composed only by Carbon atoms, and they differ by the geometric construction: diamond is a crystal with tetrahedral elemental unit, whereas graphite is a stacked honeycomb lattice.

PUC-Rio - Certificação Digital Nº 1011917/CB

For being different forms of the same element, diamond and graphite are called Carbon allotropes.

Again, given the flexibility of Carbon atom, through its hybridization capabilities, Carbon may be present even in different structures other than diamond and graphite. In laboratory it has been possible to synthesize other allotropes of Carbon: Buckyballs (of which, C_{60} is an example), Graphene, Carbon Nanotubes, Carbon Fibers, Carbon Nanohorns, etc.

What is interesting is that Carbon allotropes can be found as different dimensional quantum systems. For instance, Buckyballs might be viewed, depending on the application, as a quantum dot, that is a 0 dimensional system. Carbon Nanotubes are usually studied as 1 dimensional structure. Graphene, which is a 1 isolated graphite layer, has properties of 2 dimensional quantum systems. And finally, diamonds can be studied as 3 dimensional systems. The restricted dimensional systems (graphene, Carbon Nanotubes, and buckyballs) have usually outstanding and unusual physical properties, owing to the spatial confinement of its electrons.

Single Walled Carbon Nanotubes can be viewed as rolled graphene, and multiwall Carbon Nanotubes have the structure of many concentrically rolled graphene layers (Russian doll model). The structure of Carbon Nanotubes has firstly been unraveled by Ijima, in its seminal paper in 1991 [1].

PUC-Rio - Certificação Digital Nº 1011917/CB

2.1.3. Carbon Nanotubes: Geometry and Classification

Carbon Nanotubes can assume more than one geometry. Indeed, its physical properties, such as electronic, optical, and mechanical depend on the Carbon Nanotube structure. Thus, this chapter will present the various forms one can find Carbon Nanotubes, and name the different classifications.

The first way to classify a Nanotube is by the number of walls it has. If the Nanotube has only one wall, that is, it is composed of a single rolled up graphene sheet, it is designated as single-wall Carbon Nanotube (SWNT). If the Nanotube is composed of a superposition of more than one concentrical cylinder, it is called a Multi-Wall Carbon Nanotube (MWNT).

The picture of a Nanotube as being a rolled version of graphene brings up a question, as to how this graphene should be rolled. Figure 2 (taken from [3, p. 112]) depicts a graphene sheet, and is an example of how to understand Nanotube geometry from Graphene. The vector $\vec{T}$ represents the tube axis direction, whereas the vector C represents the tangential vector, that is, the roll up direction. The point named as $(6,3)$ will coincide with the point $(0,0)$ in the corresponding Nanotube. Given the vector $\vec{C}$, the vector $\vec{T}$ is determined uniquely, and so is the Nanotube geometry.

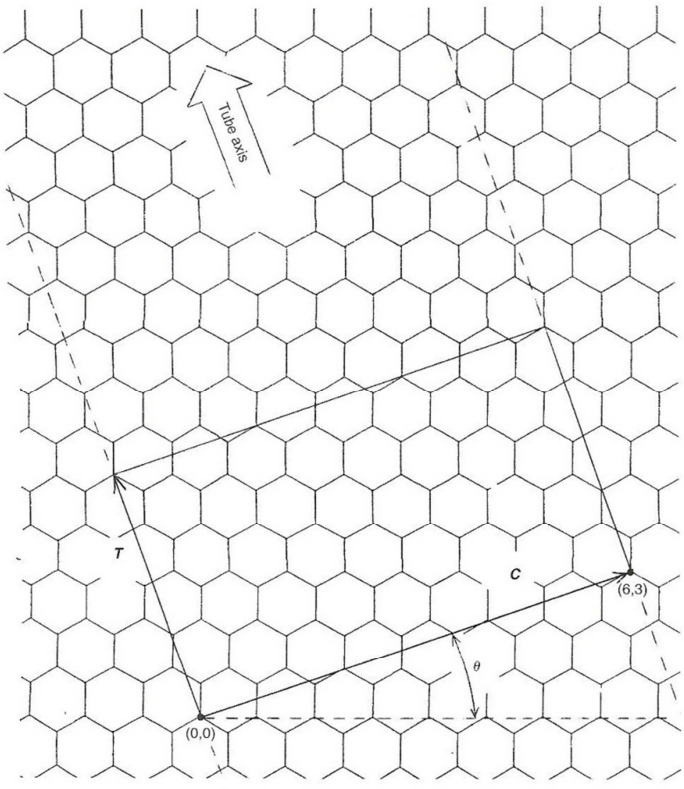

Figure 2: This figure is a possible geometry of a single-wall Carbon Nanotube (SWNT). It represents how the Nanotube structure can be understood as a rolled up version of a Graphene sheet. The vector T represents the tube axis, whereas the vector C is the roll up direction. This way the point designated as (6,3) will coincide with the (0,0) point in the SWNT.

One way to determine Nanotube geometry is by using the unit cell vectors from Graphene as reference. In

Figure 3 (from [3, p. 110]), a Graphene sheet is described as a function of the unit cells $\vec{a}_1$ (parallel to the zigzag direction) and $\vec{a}_2$ (60^o in relation to $\vec{a}_1$). The labels (n, m) give the position of a given vertex in relation to the origin $(0,0)$ in terms of a sum of $n\ \vec{a}_1$ units and $m\ \vec{a}_2$ units. Rolling the Graphene sheet in such a way that the vertex (n, m) coincides with the origin makes up a Nanotube, with roll up vector $\vec{C}$. This way, the following equation holds:

PUC-Rio - Certificação Digital Nº 1011917/CB

$$\vec{C} = n \cdot \vec{a}_1 + m \cdot \vec{a}_2 \qquad \text{Equation (5)}$$

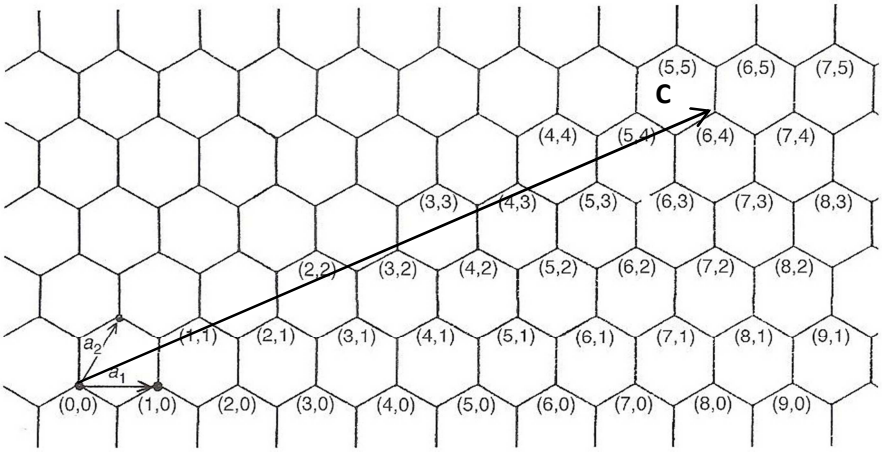

Figure 3: This figure represents Nanotube possible geometries as a function of graphene unit cell vectors. All named vertexes can be described as a sum of unit cell vectors a_1 and a_2. In the same way, the vector C can be described as a sum of the unit cell vectors: $\vec{C} = 6 \cdot \vec{a}_1 + 4 \cdot \vec{a}_2$

Since, the pair (n, m) defines the vector $\vec{C}$, the Nanotube geometry is completely determined by this pair of numbers, which is called chirality of the Nanotube. A zigzag Nanotube will be described as a $(m, 0)$ tube, and an armchair tube will have the designation of (n, n). All other tubes will be generally described as (n, m) tube, with $0 \leq m \leq n$, and are called chiral tubes. Figure 4 below, taken from [4], illustrates the geometry and depicts the $3D$ model of an armchair Nanotube, a zigzag Nanotube, and a chiral Nanotube.

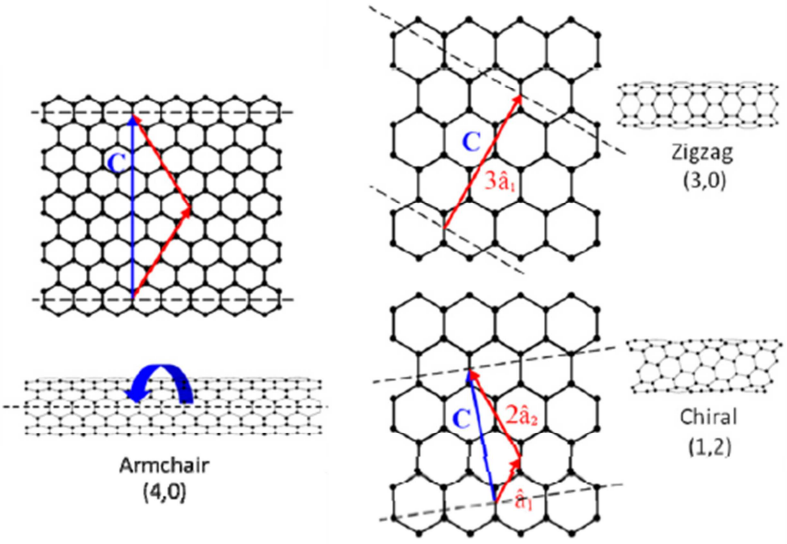

Figure 4: Geometry and $3D$ representation of an armchair tube on the left side; the same for a zigzag tube on the upper right side; a $(1,2)$ tube on the lower right side.

All geometrical parameters of the tube are derived from the chirality. For instance if one wants to calculate a specific Nanotube diameter, it must bear in mind that

PUC-Rio - Certificação Digital Nº 1011917/CB

the magnitude of the $\vec{C}$ vector is the Nanotube perimeter. Some calculation will lead to the relationship below:

$$d = a\frac{\sqrt{n^2 + n \cdot m + m^2}}{\pi} \qquad \text{Equation (6)}$$

Where, the number a bears a relation with the interatomic distance a_{C-C}:

$$a = |a_1| = |a_2| = a_{C-C} \cdot \sqrt{3} = 2.46\,\dot{A} \qquad \text{Equation (7)}$$

The equations above will be used in the Results section " RBM Mode".

The above description is useful, but it misses to describe defects that might be present on the tube walls. There are different classes of defects that change the honeycomb structure of a Nanotube, but usually they are related to the presence of a pentagon and/or a heptagon cell in place of a hexagon on the tube walls.

PUC-Rio - Certificação Digital Nº 1011917/CB

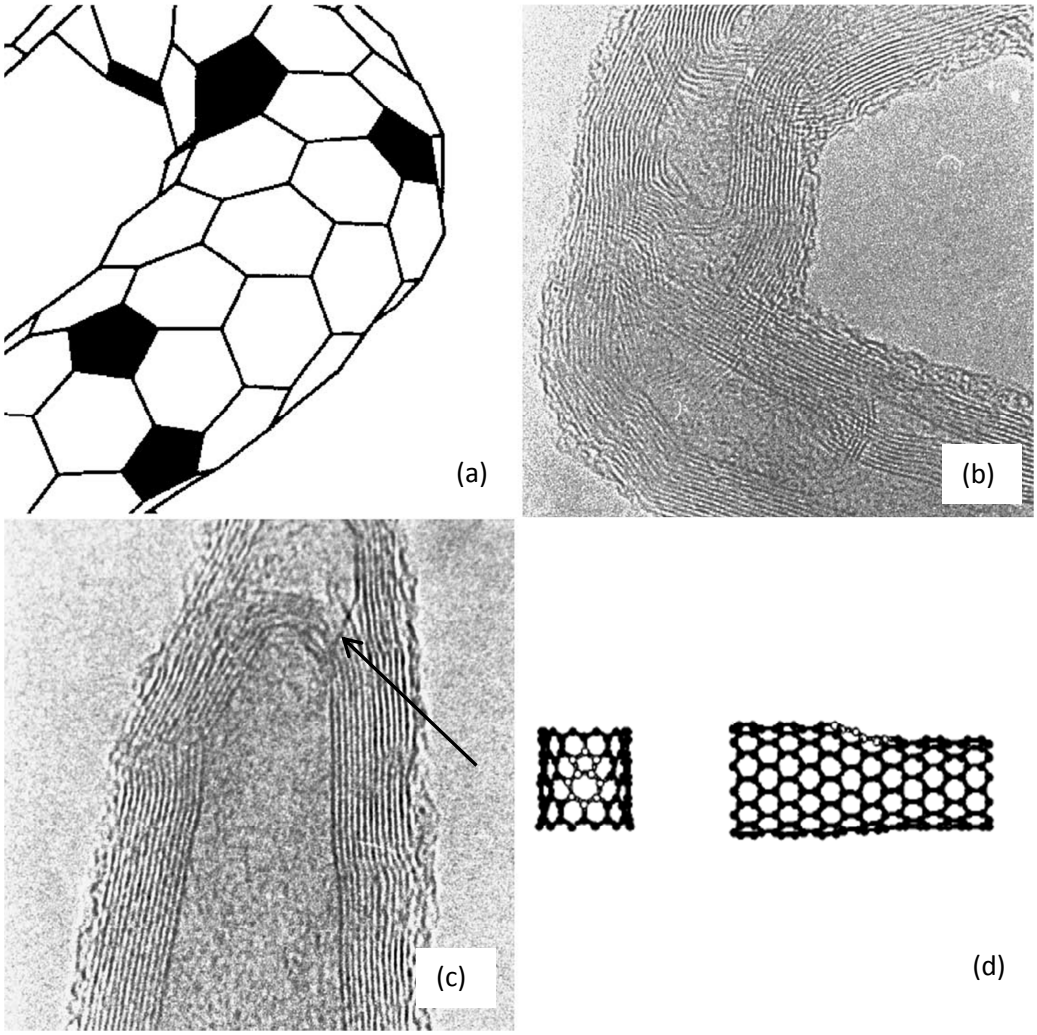

Figure 5: Examples of defects in Nanotubes. In (a) pentagon and heptagon defects responsible for the curvature in the tube. In (b), the transmission electron microscopy image of the corresponding

MWNT curved, because of the latter effect. In (c), a Nanotube cap composed of a set of defects, which are responsible for the cap curvature. In (d), a pentagon-heptagon pair. Pictures (a) to (c) are from reference [5], and picture (d) is from reference [6].

Pentagon-heptagon pairs, first studied by Charlier et al. [6], are not associated with misalignment of a tube, but has effects on its electronic properties, as well as its chemical stability, for it increases locally the energy per atom and stretches the $C - C$ bonding distance. Another type of defect, tube junctions happens due to the presence of pentagon and heptagon defects on opposing sides of the tube walls and tend to bend the tube, thus being responsible for the experimental observation of curved and curly Nanotubes.

Wall structural defects are related to reorganization of C atoms, in such a way to change the usual honeycomb type structure. The defects are related to a decreased chemical stability of Nanotubes, meaning that they turn more amenable to chemical reactions. Defects are also responsible for changes in electronic properties for representing a symmetry break along the tube axis.

In the Figure 5 (taken from [5], and [6]), it can be seen examples of the effect of defects on the structure of Nanotubes.

Another effect of defects is tube capping. The tubes are usually found with a cap, and the caps are composed basically of defective cells (pentagons and heptagons), which are responsible for the necessary curvature to close the Nanotube ends. This way, defects may sometimes be related to termination of growth of Nanotubes, and an increase in tube defects usually will result in shorter tubes. This has direct impact in the discussion about doping of Nanotubes, as will be seen latter because doping itself represents a defect on the tube walls.

A final effect of defects, which is observed specially in doped Nanotubes, is the existence of bamboo-like structures in MWNTs. These structures consist of capping of the inner tube walls before the end of the tube.

Examples of defects in Nanotubes produced in this thesis are shown below.

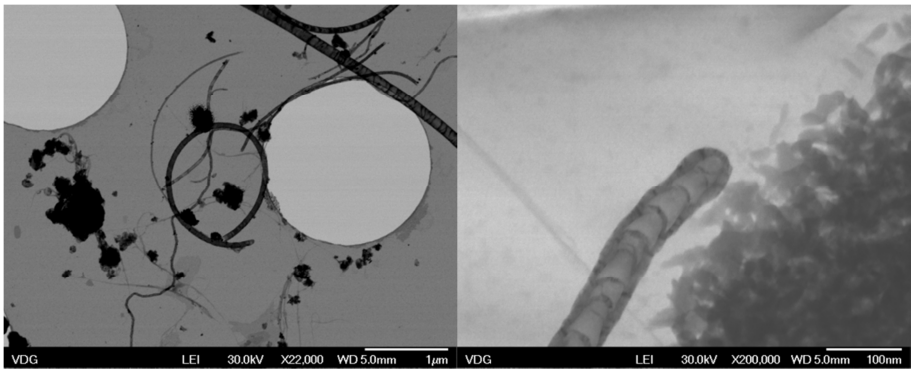

Figure 6: These are examples of Nanotubes produced in this thesis, showing some kind of defect. The left picture shows a curving MWNT. This effect is caused by pentagon and heptagon defects in opposing sides of the tube. The right picture shows a bamboo-like MWNT. The bamboo-like Nanotube occurs might occur as a consequence of doping.

The concepts and terms introduced here will be used in the next chapters to describe the Nanotube physics, and later to discuss the experimental results.

PUC-Rio - Certificação Digital Nº 1011917/CB

2.1.4. Types of doping

This thesis is concerned about synthesizing and characterizing doped Carbon Nanotubes. Thus, this section is devoted to give a general idea of what doping is.

There are three types of doping essentially: exohedral doping, endohedral doping, and in-plane doping (classification from [7, p. 531]). It will be explained each of these types.

2.1.4.1. Exohedral doping

Atoms and molecules may reside in between Nanotubes in Nanotube soots. These elements, or molecules, will function as electron donors or acceptors, and the Carbon Nanotube will be said to be doped. This type of doping is also known as intercalation.

Reference [8] demonstrates the functionalization of Carbon Nanotubes by chemically attaching radical groups, such as $-COOH$ to the outside Nanotube walls, by prior acid treatment, as depicted in Figure 7, taken from [8].

The exchange of charge carriers will influence Raman spectra causing a downshift (upshift) in frequency when electrons (holes) are given away to the tube. Absorption spectra will also change making some bands disappear and others appear. At last, decrease in resistance might be observed, given the increase in the number of charge carriers in the Nanotube.

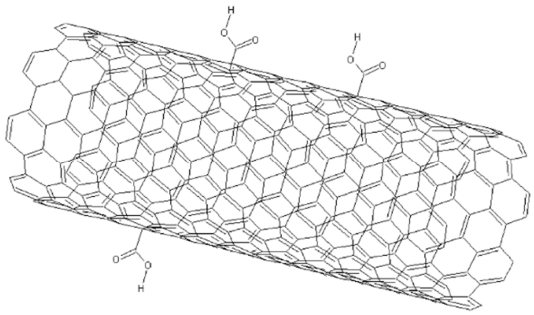

Figure 7: Illustration taken from [8], shows –COOH groups anchored onto a Single Walled Carbon Nanotube.

2.1.4.2. Endohedral doping

The experimental discovery of Nanotube capillarity by Ajayan and Iijima [9], opened the possibility of encapsulating atoms, molecules and crystalline materials inside a Nanotube. The presence of such chemical substances inside Nanotubes is known as endohedral doping, or filling.

A significant step in this direction was the discovery of peapods, which consist in encapsulating buckyballs molecules (for example, C_{60}) inside SWNTs. Reference [8] demonstrates the possibility of C_{60} and C_{70} filling of SWNTs. Figure 8 shows a Transmission Electron Microscope (TEM) image, in which a Nanotube filled with Buckyballs can be observed.

PUC-Rio - Certificação Digital Nº 1011917/CB

This Nanotube filling possibility unravels the possibility of making chemical reactions in an isolated and controlled way inside the Nanotubes. In [8], for example, the polymerization of fullerenes inside SWNTs and the formation of double-wall Carbon Nanotubes from peapods are demonstrated. Nanotubes have been used to study the behavior of water molecules inside nanochannels, proving the possibility of utilizing such Nanotubes as nanoreactors [10].

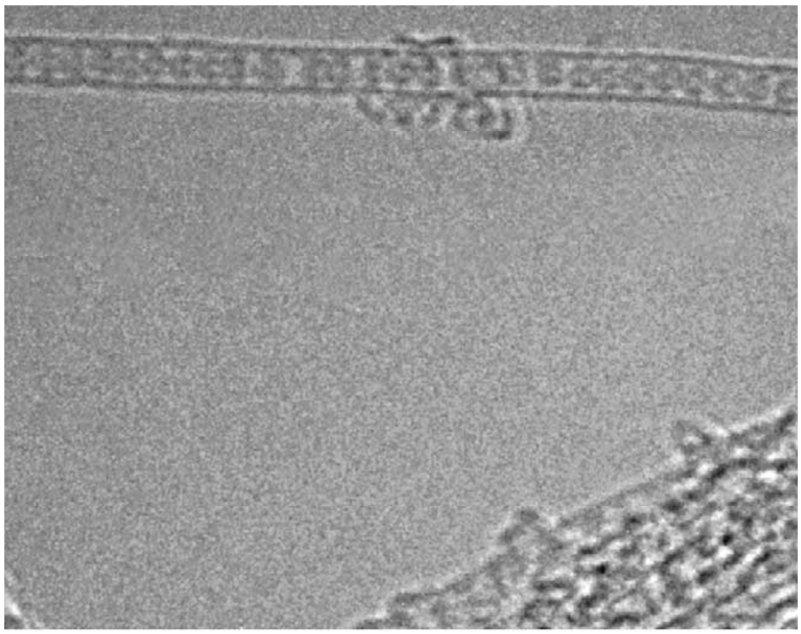

Figure 8: In this TEM image, taken from work [8], it can be seen a Nanotube filled with buckyballs, which can be identified as circular features inside the cylindrical structure of the Nanotube.

2.1.4.3. Substitutional doping

The presence of heteroatoms on the Nanotube walls, occupying a Carbon atom site is known as in-plane, or substitutional doping. In this thesis, the focus will on be substitutional doping, since the main objective is to synthesize substitutionally Boron doped SWNTs. So a better understanding of this kind of doping is necessary.

Specifically Boron will be present in the Nanotube lattice as a 3-coordinated atom, that is, it will be bonded to 3 neighboring Carbon atoms, which is the coordination of the Carbon atoms themselves. Thus, the presence of B atom will not create heptagon or pentagon type defects, although it will weaken the Nanotube structure locally, since $\mathrm{B-C}$ bonds are weaker than $\mathrm{C-C}$ bonds. Figure 9 is a picture, adapted from [11], showing the structure of BC_3 islands in Boron doped Nanotubes.

Doping with Boron is said to be p type as B atom will accept electrons (donate holes) from (to) the Carbon Nanotube's valence band. The presence of this element in the Nanotube lattice will create electronic states right above the valence bands, lowering, thus, the Fermi level, and this will have direct consequences in the transport properties, optical properties, and Raman spectra of B-doped Carbon Nanotubes as will be seen latter.

PUC-Rio - Certificação Digital Nº 1011917/CB

For comparison sake, Nitrogen in-plane doping can admit two types of coordination, as the N atom can occupy two different places in the Carbon Nanotube walls: it is said to be “substitutionally” doping, when assuming a three coordinated position, like C atoms; and it is said to be “pyridinically” doping when assuming a two coordinated position. In “pyridinic” doping, a first neighbor C atom is missing from the structure.

In the first case, Nitrogen doping will be n-type, that is N atoms will donate electrons to the conduction band, and, as a consequence, will increase the Fermi level. In the second case, N atoms can both donate electrons to the conduction band, or accept electrons from the valence band: the n or p type character of the doping will depend on the number and geometric position of N atoms.

In plane doping play a role on the structural integrity of Carbon Nanotubes. It has been reported, [12,13,14], that the presence of heteroatoms in the growth of Carbon Nanotubes, will increase the degree of disorder, and produce shorter tubes ([14]), although there is not a complete agreement on this topic, [15,16,17]. In [15], the authors observe no evidence for increased disorder within their analysis method (Raman Spectroscopy), although agrees with the otherwise expectation. [18] and [17] report increase in c-axis ordering (normal to the tube walls), although [18] agrees with decrease in tangential ordering.

Concluding, in-plane doping is achievable with other elements, for example, [19] produces and characterizes Phosphorus doped MWNTs.

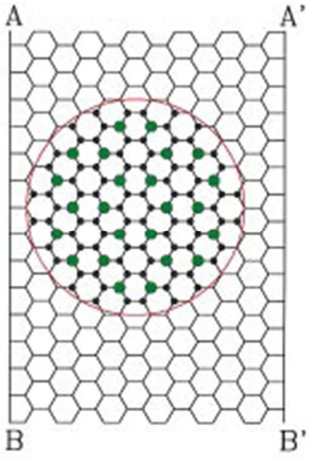

Figure 9: Picture adapted from [11], is an example of substitutional doping of Nanotubes with Boron. In the picture, the black circles are Carbon atoms, while the green ones are Boron atoms, which assume in the Nanotube structure the place of Carbon atoms. The authors observe in their doped Nanotube samples the appearance of BC_3 islands.

2.2. Carbon Nanotube Synthesis: an overview

As seen in the previous sections, Carbon Nanotubes are Carbon allotropes with peculiar cylindrical 1D structure, with various geometries which depend on the tube chirality.

Since, the tube properties depend upon the tube chirality, a selective production would have been advantageous in understanding Carbon Nanotube Physics deeper. Notwithstanding, the Carbon community is still seeking to control the

PUC-Rio - Certificação Digital Nº 1011917/CB

synthesis of Carbon Nanotubes, and to do so it is necessary to understand the growth mechanism of such macromolecules.

In this section, the synthesis techniques used to produce Carbon Nanotubes will be shortly described, and a review of the scientific community knowledge about Carbon Nanotubes' growth mechanisms will be presented.

In the first part of the section, the synthesis techniques and growth mechanism for pristine tubes will be presented. On the second part, the production of doped tubes will be addressed.

2.2.1. Pristine Carbon Nanotube

In this section, it will be reviewed some of the advances in the area of synthesis of Carbon Nanotubes, in pristine form, that is, not doped.

In a general sense, Carbon Nanotubes synthesis can be grouped in three general methods: arc discharge methods, laser ablation methods, or chemical vapor methods. These methods will be discussed separately in the following sections.

2.2.1.1. Arc-discharge production of Nanotubes

On seminal paper by Iijima, on the discovery of Carbon Nanotubes [1], the author describes that his material was produced in an arc-discharge method, so this method has historical importance to the field. In this method, a vacuum chamber has a pair of graphite electrodes, impregnated by a given metal, which will work as a catalyst. During synthesis, a flow of inert gas fills the chamber and a high voltage between the electrodes promotes discharge, which vaporizes the metal catalyst together with Carbon material. As a product, the walls and the electrodes will be impregnated with deposited Carbonaceous material that, under the right conditions, will contain Nanotubes. Figure 10, taken from [20], presents a schematic of the apparatus used by the paper authors to produce SWNT by arc discharge, and the Nanotube material produced.

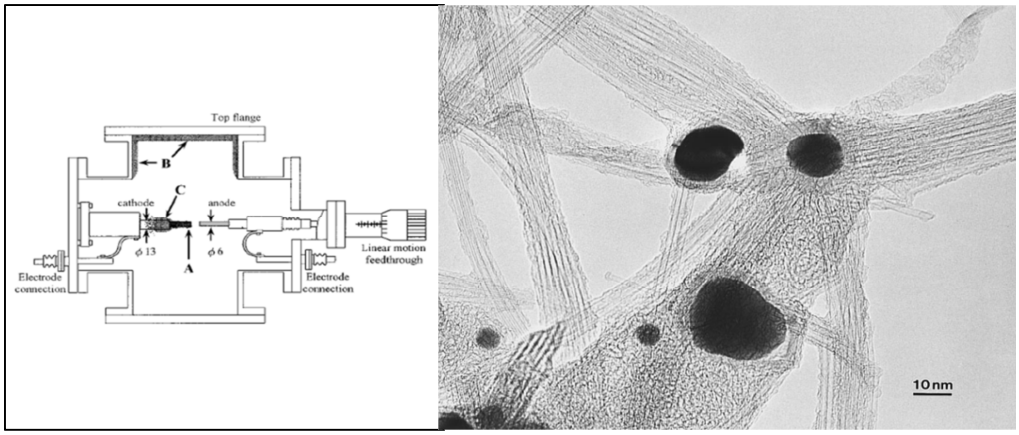

Figure 10: An example of arc discharge method. On the right-side panel, a schematic of the apparatus, and on the left-side panel, the material produced.

PUC-Rio - Certificação Digital Nº 1011917/CB

2.2.1.2. Laser vaporization production of Nanotubes

In the laser vaporization method, a metal doped graphite target usually heated to around $1000\ ^oC$ temperature is hit by a laser under inert gas flow. Some material is produced and collected in a cool collector. Although, the SWNT produced has almost no by-products, the rate of production is low, around a gram per day.

2.2.1.3. Chemical Vapor Deposition production of Nanotubes

The last method for producing Carbon Nanotubes is called chemical vapor deposition (CVD), and is seen as a promising method for commercial production of Carbon Nanotubes, in contrast with the others, for its ability to be scaled up to high rates of production, together with its controllability. As this thesis uses CVD method to synthesize its material, more focus will be given to it.

The CVD method has many variations, and some examples will be given, but the main idea is conveying one or more substances in vapor phase to a reactor, which is held at some specified temperature, where it will react, and be deposited, either in the reactor walls, or a crucible, or even a flat substrate.

The metal catalyst can be conveyed in the vapor phase or it may be kept inside the reactor, in solid form from the beginning of the reaction. The source of Carbon atoms is introduced in the reactor in the form of organic substances in vapor phase. The source of Carbon is usually called the precursor. An important parameter here is the rate of flow of the precursor, or the partial pressure of the precursor, depending on the specific CVD apparatus.

Either before or simultaneously with the precursor flow, an inert gas and/or a reducing gas flow is introduced into the reactor. The flow rate or the partial pressure of the inert or reducing gas is another important parameter in CVD technique.

The temperature of the reactor is one of the main parameters of this method of synthesis, together with gas/vapor pressure. Usual temperatures vary from $500\ ^oC$ to $1000\ ^oC$, and pressures vary by many orders of magnitude, for some groups synthesize under atmospheric pressure with high yield of Carbon Nanotubes, while others under low vacuum to high vacuum pressures, with lower yield.

One of the CVD methods is the spray pyrolysis method, [21], [13], [22], and [23]. Within this method, the catalyst is not on a substrate in the reactor, but it is conveyed with the precursor in the form of a spray carried by some inert gas. In references [21] and [13], an Iron containing compound (ferrocene) is dissolved in toluene and carried by argon gas to the reactor. Temperatures used are in the range of approximately $600\ ^oC$ to $800\ ^oC$, and flow rates are controlled by the flow rate of Argon gas, and the concentration of ferrocene in toluene. In [22], Iron nitrate is dissolved in water, and carried by N_2, whereas the precursor is delivered to the reactor in gas form (C_2H_2, acetylene). In [23], ferrocene is dissolved in benzene, and carried with argon gas into the reactor at $700\ ^oC$ to $900\ ^oC$ (actually a two-step furnace is used, but the reactor stage is used in the $700\ ^oC$ to $900\ ^oC$).

Another common form of CVD is supported catalyst CVD, in which the catalyst is deposited prior to synthesis on a substrate and laid inside the reactor. Basically,

PUC-Rio - Certificação Digital Nº 1011917/CB

one can distinguish two types of supported catalyst in the literature: thin film catalysts ([24], [25], [26]), and powder catalysts ([27], [28], [5]).

In the case of thin film catalyst, a thin layer of the catalyst is deposited over a flat surface. The flat surface may be silicon oxide ([26] , monocrystalline magnesium oxide, quartz, aluminum oxide, zeolites (aluminum silicates) etc. And the thickness may vary from roughly $100\ nm$ to discontinuous subnanometer films. When powder catalysts are used, metal catalyst impregnates some micro or nanoporous powder made of alumina (fumed alumina Degussa) or magnesium oxide usually.

In this thesis, supported catalyst high vacuum CVD has been employed. High vacuum CVD means that prior to deposition, high vacuum conditions are applied to the reactor to assure an oxygen-free ambient and the deposition occurs at slow rate and low vacuum pressures. As it will be further discussed in the Experimental section, it is used a liquid precursor, whose vapor enters the reactor, held at high temperatures. Prior to the deposition, a H_2 flow is established to reduce the metal catalyst, an Iron impregnated Magnesium Oxide powder (supported catalyst).

2.2.1.4. Growth mechanisms of Carbon Nanotubes

PUC-Rio - Certificação Digital Nº 1011917/CB

One of the main barriers for the Carbon community to objectively engage the question about the feasibility to selective grow Carbon Nanotubes is the understanding of the atomic dynamics underlying Carbon Nanotube growth. Indeed, there is not a complete agreement about the mechanism by which Carbon atoms gather to form a Nanotube. In this section, the mechanisms used to explain Carbon Nanotube growth will be discussed.

The different synthesis methods are explained within the frame of different growth mechanisms. For example, solid state models [3, p. 22 and 34] were used to explain production of Single Walled Carbon Nanotubes in laser vaporization experiments: solid carbon particles would agglomerate before their conversion into Carbon Nanotube by the catalyst particle. On the other hand, the most used model, mainly within Chemical Vapor Deposition synthesis, is known as vapor-liquid-solid. Since CVD is the synthesis technique used in the present thesis work, this growth model is especially important.

Vapor-liquid-solid mechanism (VLS) was first used to explain the formation of Si, Ge and other materials whiskers. Later, Tibbetts et.al. [29] used this mechanism to explain the catalytic growth of Carbon Nanotubes.

In the VLS model, the precursor is considered to decompose under the synthesis conditions to give place to a Carbon atom vapor, at the same time the metal catalyst forms nanometric-sized liquid droplets. The Carbon atoms diffuse into the catalytic particle, and tend to form a sp^2 web on its surface. For reasons like surface irregularities, or thermal agitation, etc. this web detaches from the catalytic surface and keeps growing, as more Carbon atoms diffuse into the catalyst and attaches to the edges of the Carbon web. Figure 11, taken from [30] illustrates the aforementioned process.

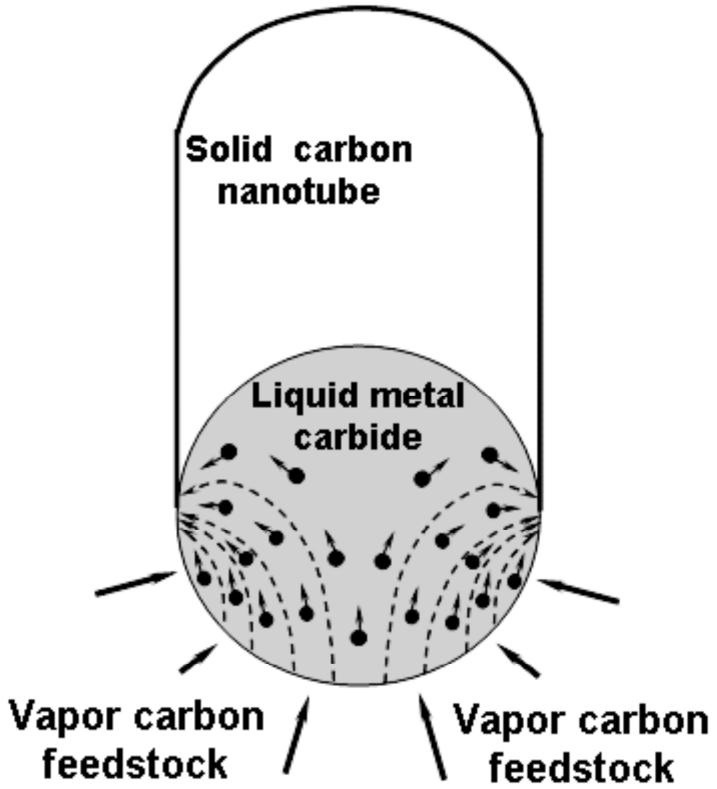

Figure 11: This Picture, taken from [30], illustrates the growth mechanism in the VLS model. The Carbon atoms from the feedstock diffuse into the liquid catalyst particle, and attach to the edges of the growing Nanotube.

Many aspects are still unclear within the VLS model. For example, in the case of Multi Walled Carbon Nanotube growth, the catalytic particle, which has size comparable to the Nanotube diameter (some nanometers), cannot physically be in the liquid state, under synthesis conditions, thus violating one of the hypothesis of the VLS model.

Another matter of discussion is the driving mechanism for the diffusion of Carbon atoms in the metallic particles. Concentration gradients seems to be the driving force responsible for the carbon atoms to go from one free side of the catalyst particle to the other, and feed Nanotube growth.

The formation of a graphene-like web on the metallic catalyst surface seems to indicate that only metals with mild Carbon solubility should be good catalysts for Carbon Nanotube growth. On the other hand, there are reports on the growth of Carbon Nanotubes using various catalyst materials [24], including Cu, which is known to form alloys with Carbon.

Another question is about tip or base growth, that is, whether the Nanotube sticks to a support material while the catalyst is driven away by the Nanotube growth, or whether the catalyst particle sticks to a support and the Nanotube grows away from it. There are evidences for both the mechanisms, and it seems the metal-support interaction force is the main factor.

PUC-Rio - Certificação Digital Nº 1011917/CB

2.2.2. Substitutional Doped Carbon Nanotubes synthesis

The basic synthesis methods used for pristine Carbon Nanotubes are also used, in an adapted way, to synthesize doped Carbon Nanotubes. In this section, it is introduced in a general way, how the doped Carbon Nanotubes have been produced in the Nanotube scientific community. Focus will be given to Boron doped Carbon Nanotubes.

In the arc discharge method, doped Carbon Nanotubes can be synthesized by doping the graphite electrodes with the corresponding doping material. For example, in [17] and [18], either B or BN are added to the graphite electrodes to yield Boron doped MWNTs. X-Ray Diffraction analysis of Boron doped MWNTs present higher crystallinity, and a preferential zigzag geometry [16]. It is also identified that some Boron carbide (B_4C) by-products. Arc-dischard method is used to produce $B-C-N$ and Boron doped Nanotubes with evidence of improved crystallinity in graphite c direction [27].

In [31] and [32], Boron doped single-wall and double wall (DWNT) Carbon Nanotubes are produced by laser ablation method, when doping the Carbon target with elemental Boron. The levels of doping are undetectable in [31] (limited in the upper limit to $0.1-0.05\ at.\%$) by the analysis method used by the authors (Electron Energy Loss Spectroscopy, EELS), which is a recurrent problem when producing B doped Carbon Nanotubes with Boron concentration below $1\ at.\%$. In [32], an indirect evidence for the presence of Boron on the SWNT structure is achieved by measuring electrical properties (thermo power measurement).

Another way to produce Boron doped Carbon Nanotubes is the so called substitution method. In it, pristine Carbon Nanotubes are placed in a reactor, and exposed to Boron containing molecules (for example, B_2O_3, at high temperature [30]. Boron substitutes Carbon atoms on the Carbon Nanotube lattice, and high doping levels are achievable. Boron concentrations as high as $10\ \%$ [30], and $15\ \%$ [31] are produced by substitution reaction method.

CVD methods can also be applied do B doping of Nanotubes. In particular, doping of MWNTs is discussed by many authors [12,14,33].

In [33], MWNT doped by both Boron and Nitrogen is produced using as precursor Methane, and introducing diborane (B_2H_6) in the flow, together with N_2, and H_2 The pressure in the reactor is around $22\ torr$, and temperature in the substrate (Nickel policrystaline wafers) is $620\ ^oC$, and the experiment is a variation of the Chemical Vapor Deposition method. Its peculiarity is the application of a high voltage bias between substrate and a filament, which imposes an alignment in the synthesized tubes, and renders the technique the designation bias assisted hot filament CVD.

In [12], the precursor, Ethanol (C_2H_5OH), is introduced into the reactor with Boron oxide (B_2O_3), which is carried by H_2 from a Water/Ethanol solution, to produce Boron doped MWNTs.

Multi Walled Carbon Nanotubes are produced using as precursor Methane (CH_4), and as Boron source Trimethyl Borate ($B(OCH_3)_3$) [14]. It is noted that the amount of defects of the Nanotubes increase with increasing Boron content (in contrast to what [17] finds), and that the length of the tubes shorten. The same

PUC-Rio - Certificação Digital Nº 1011917/CB

substance, Trimethyl Borate is proposed as possible B sources for the production, not of MWNTs, but SWNTs.

Reports on the production of Boron doped SWNT, using the CVD method it can be found, in many references [15,34,35,36]. The Dresden group reports the production of B doped SWNT using a single substance as both precursor and Boron source, Triisopropyl Borate ($B(OC_3H_7)_3$). In our group [35,36] we investigate the substitution of Triisopropyl Borate by Triethyl Borate ($B(OC_2H_5)_3$) in the synthesis of doped Carbon Nanotubes, comparing the production of SWNT using these two different substances as precursors at different temperatures.

The works on Boron doping using Trimethyl, Triethyl, and Triisopropyl Borate inspired this thesis, whose objective is to evaluate the feasibility to control and quantify doping levels for Boron doped SWNTs using different precursor substances, and their mixture. The fact that the three substances come from the same class of alkyl Borates, and thus have similar physical and chemical properties was seen as an attractive when planning the thesis, because less uncertainties would be present when comparing the synthesis results

As this thesis aims at the feasibility of controlling Boron doping levels for SWNTs prepared by CVD, the paper [37] also has special importance, for it succeeds in producing different doping levels by changing the precursor to B source feed rate. The authors performed an extensive characterization of the resulting material using X-Ray Diffraction, X-Ray Photoelectron Spectroscopy, and Raman Spectroscopy.

2.3. Analysis Techniques

In this chapter, a background will be introduced to the techniques used to analyze the material synthesized in this work. From this chapter, the reader will grasp the basic theory necessary to understand the discussion of the experimental results.

2.3.1. Raman Spectroscopy

In atomic Physics [38], there is a brief discussion about the difference between elastic scattering of a photon by an atomic or molecular system, which is termed Rayleigh Scattering, and inelastic scattering of a photon by an atomic or molecular system, which is called Raman Scattering. In the first process, the incident and the scattered photon have the same energy, meaning that the initial and final state of the atomic or molecular system is the same (or at least has the same energy). In the second process, it is mandatory that the atomic/molecular initial and final states are different in energy, because the incident and emitted photon have different energies.

In both processes, there is an intermediate state to which the system gets excited to. The tuning between the incident photon energy and the energy gap between the initial and the intermediate state, or the tuning between the out coming photon and the gap between final and intermediate state characterizes what is called a resonance, when the cross-section for the process is maximized. Equation (8), adapted from [38, p. 231, eq. 4.227] grasps the main aspects of Raman effect,

PUC-Rio - Certificação Digital Nº 1011917/CB

although it is not exactly the same equation used by M. Dresselhaus in [39], for it does not account for the out coming photon resonance.

$$\sigma_{fi} \propto \frac{E_i {E_f}^3 M_{fnni}}{(E_i - E_{ni})^2 + \left({}^{h}/_{2\tau}\right)^2} \qquad \text{Equation (8)}$$

On the above equation, σ_{fi} is the total cross-section for the Raman scattering to happen between atomic/molecular initial state i, and final state f. From Equation (8), σ_{fi} depends on the incoming photon energy E_i, on the scattered photon energy E_f, on the energy difference between the initial and the intermediate state E_{ni}, on the intermediate state life-time τ, and on the term M_{fnni}, which is the total matrix element for the process, squared and integrated over all angles.

From the Equation (8), it can be seen that, when the incoming photon has the same energy as the energy gap E_{ni}, the process intensity will be maximized. Furthermore, the M_{fnni} term imposes the, so called, selection rules, which are related to symmetries of the systems; only processes related to non-zero M_{fnni} might happen.

Based in this concept, Resonant Raman Spectroscopy is a technique in which a sample is excited by a laser in the visible range, and the outcoming light, is analyzed in wavelength domain. The intensity vs. Raman shift (which is given in the Equation (9)) plot gives information about the vibro-rotational modes of the sample.

$$\Delta\omega\ (cm^{-1}) = \left(\frac{1}{\lambda_i} - \frac{1}{\lambda_f}\right) \times 10^7,\ \lambda(nm) \qquad \text{Equation (9)}$$

It must be stressed that usually the laser energies used for Raman spectroscopy are in the visible range, so they have energies of the order $\sim 1\ eV$, which is the order of magnitude of electronic transitions, and that usual energy difference between incoming and scattered photons is in the sub eV range (infrared range), which is the order of magnitude of vibro-rotational transitions [40]. Thus, not only will Raman spectra depend on the mechanical properties of molecules, but it will also depend on the electronic properties of materials.

In the case of Carbon Nanotubes, one is interested in relating the vibrational modes of the sample, investigated by Raman Spectroscopy, with structural and geometrical parameters of the tubes, such as for example, $C - C$ bond distance and strength, crystallinity of the tube walls, and chirality, and diameters.

In the special case of doped Carbon Nanotubes, Raman spectra is used to characterize the effects of doping type and concentration on both mechanical and electronic properties of Carbon Nanotubes, as will be explained later.

PUC-Rio - Certificação Digital Nº 1011917/CB

2.3.2. X-ray Photoelectron Spectroscopy

By shining a sample with photons, other than scattering of the photon, another, and yet more intense process that might occur, is absorption. When absorbing a photon's energy, an electron will get excited to a higher energetic state, and if necessary energy is given to the electron (energetic enough photon) it will be freed from the atom.

X-ray photoelectron spectroscopy uses this fact, in a way that within this technique, one shines a sample with photons at the X-ray range, and then observes the kinetic energy of the outcoming electrons. Equation (10) shows a direct relation between the energy of the outcoming electron, and its binding energy:

$$U = E_{ph} - K \qquad \text{Equation (10)}$$

In the above equation, one can calculate the binding energy U, from the kinetic energy K, given the photon energy E_{ph}. By making a plot of number of electron counts by binding energy, one has information of the atomic structure of the materials.

In an X-ray Photoelectron Spectrum, it will be identified peaks corresponding to each core orbital of each element present in the sample (see [41] for a guide on elements spectra). Since the innermost electron orbitals in the atoms are negligibly influenced by the neighboring atoms, it can be measured the relative amount of each element in a sample by probing these orbitals.

On the other hand, some elements, less electronegative, may allow some shift in binding energy even of its inner orbitals, depending on the element it is bonded to, and on the hybridization of its valence electrons. As a result, if an element occurs in a sample with different bonding environments, each one will produce different replicas of this element's peak shifted in relation to the ideal isolated atom's peak position by a few eV. It will be seen in the experimental section how a XPS should be interpreted in order to give quantitative results, taking into account the aforementioned effect.

When doping Carbon Nanotubes, XPS is an important tool to distinguish the amount of Boron bonded to the Nanotube walls to the amount of Boron in other compounds. This way, XPS can be used to calculate the amount of doping.

2.4. Physical Properties of Carbon Nanotubes

So far, it has been described the general structure of Carbon Nanotubes, how they are grown, and how they are characterized (at least to the extent of the present work). In this section, it will be introduced the physical properties of Carbon Nanotubes that are relevant to the discussions of the experimental results obtained in this work. It will be first presented the electronic properties, then the optical properties, and at last the Raman spectra of Carbon Nanotubes. As will be seen these properties are deeply inter related.

PUC-Rio - Certificação Digital Nº 1011917/CB

This section is divided in two: in the first part, physical properties of pristine Carbon Nanotubes are discussed; in the second part, they are compared to physical properties of doped Carbon Nanotubes.

2.4.1. Physical properties of pristine Carbon Nanotubes

2.4.1.1. Electronic properties

The picture of a Carbon Nanotube as being a rolled up version of a graphene layer, in the case of a SWNT, or of few layered graphite, in the case of MWNT, makes one wonder if Carbon Nanotubes inherit graphene or graphite's physical properties. Indeed, to study electronic and transport properties of Nanotubes, it must be understood graphene/graphite's properties.

Electronic band structure and transport properties of graphite has been theoretically described since 1947 in a seminal paper by Wallace, [42], and then revisited many times, for example in [43]. It is understood that graphene electronic structure is a good approximation to graphite electronic structure, for the interlayer distance in a graphite lattice ($0.335\ nm$) is higher than the in-plane $C - C$ distance ($0.142\ nm$).

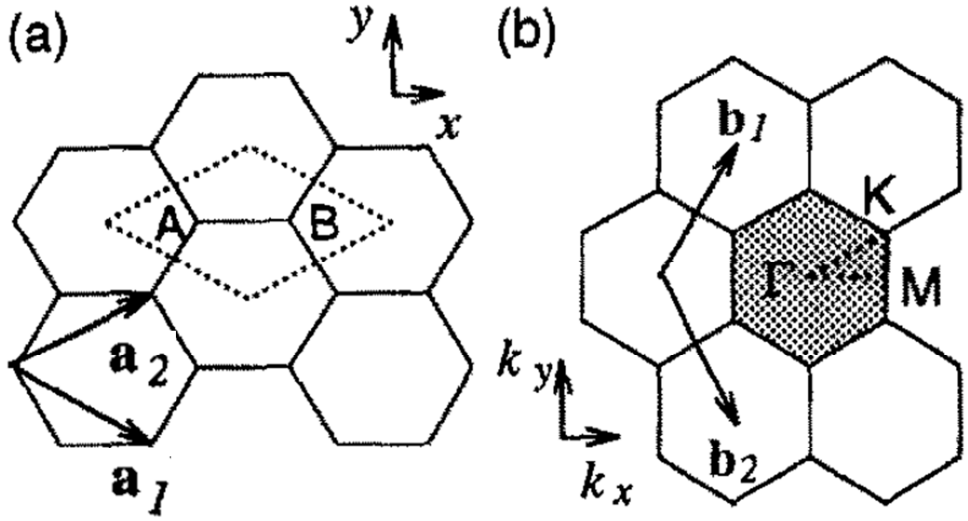

Figure 12: This figure, modified from [44], shows the coordinate system in which Equation (11) is written in. In (a), the graphene structure on position space. In (b), the same structure but in wave vector space, and in hashed the first Brillion zone.

A comprehensive and didactic explanation of graphene band structure can be found in [44]. Energy-wave number relationships (or dispersion relationships) have being described, and it is proven that graphene presents zero band gap between valence and conduction bands for the π orbital. It is considered a zero-band gap semiconductor.

Equation (11) shows the dispersion relation for graphene's π orbital, and Figure 12 (modified from [44]) shows the coordinate system in relation to which this

PUC-Rio - Certificação Digital Nº 1011917/CB

equation has been written; note that the honeycomb lattice in Figure 12 is rotated in relation to

Figure 3. E_{2p} is the binding energy of a $2p$ orbital of an isolated Carbon atom, and a_{C-C} is the $C-C$ bond distance ($0.142\,nm$), and t is known as the overlap integral for it is the overlap between neighboring C atoms π orbitals. The plus and minus solutions correspond to the conduction, and valence bands of π orbital, respectively.

$$E_{\pm} = E_{2p} \pm t\sqrt{1 + 4\cdot cos^2\left(k_y\frac{\sqrt{3}a_{C-C}}{2}\right) + 4\cdot\cos(k_x\frac{3a_{C-C}}{2})\cdot cos\left(k_y\frac{\sqrt{3}a_{C-C}}{2}\right)} \quad \text{Equation (11)}$$

At the K point, $(k_x, k_y) = \left(\frac{2\pi}{a_{C-C}}, \frac{2\pi}{a_{C-C}3\sqrt{3}}\right)$, the plus and minus solutions in Equation (11) collapse to the same value E_{2p}, proving the zero band gap at the K point. In Figure 13, adapted from [44], a plot of Equation (11) as a function of k_x and k_y (on the left panel) shows the conduction band (upper surface), and the valence band (lower surface); on the right panel, a section of the surface, taken along the high symmetry points of graphene Γ, M and K. π^* and π are the conduction and valence bands, respectively.

Although the band gap is zero, the number of electrons excited to the conduction band is low, 2.5×10^{-4} charge carriers per atom at room temperature (from [42]). This low concentration of charge carriers makes graphite and graphene to be considered also as a semimetal.

To understand the band structure of a single-wall Carbon Nanotube, and then of a multi-wall Carbon Nanotube, one usually makes the zone-folding approximation, that is, uses the same dispersion relation for graphite, but takes into account the spatial confinement in the tangential direction, by restricting the allowed wave vectors. In other words, given a single-wall Nanotube, it is finite in its tangential direction $\vec{C}$, and a graphite eigenfunction is only allowed in a given Nanotube if it satisfies the boundary condition:

$$\vec{k}\cdot\vec{C} = 2\pi n, \quad n\ integer \quad \text{Equation (12)}$$

The above equation makes the energy dispersion from Equation (11) depend on a continuous variable, and a discrete variable (n from Equation (12)), as if from the energy surface (Figure 13), one took a discrete number of sections, or branches.

Figure 14 illustrates the effect of the boundary condition, Equation (12), using a zig-zag (6,0) tube as an example: the chiral vector $\vec{C}$ is drawn in blue, and in the lower inset, the wave vector space is represented, with the allowed wave vector branches drawn in yellow, and one example of an allowed wave vector drawn in red.

PUC-Rio - Certificação Digital Nº 1011917/CB

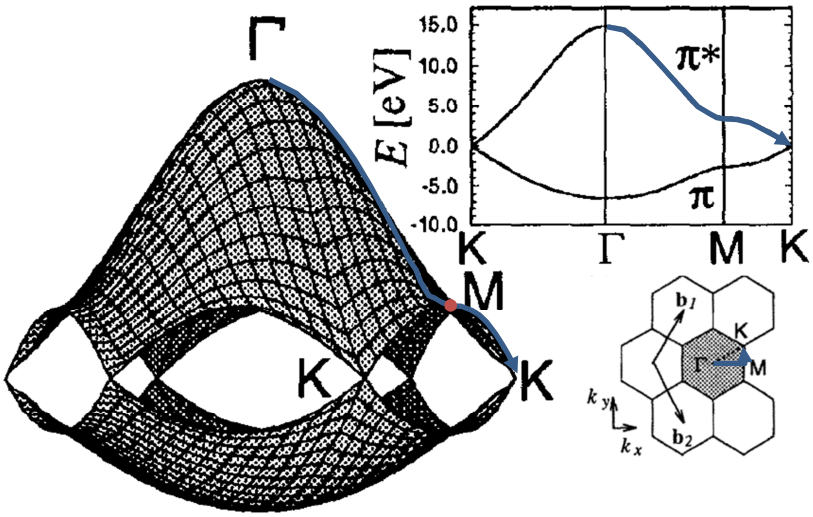

Figure 13: This figure, adapted from [44],is a drawing of dispersion relation in Equation (11). The left picture is a surface graph of the conduction (upper surface), and valence (lower surface) as a function of k_x and k_y. On the top right picture, a section of the dispersion relation taken along the symmetry points Γ, M, and K (along the blue line depicted both on the right panel and on the lower inset of the right panel).

PUC-Rio - Certificação Digital Nº 1011917/CB

It can thus be understood that if none of the allowed vector branches crosses the *K* point there will be a finite gap between the valence and conduction band. On the other hand, if at least one of the vector lines crosses the *K* point, then there will be a zero gap.

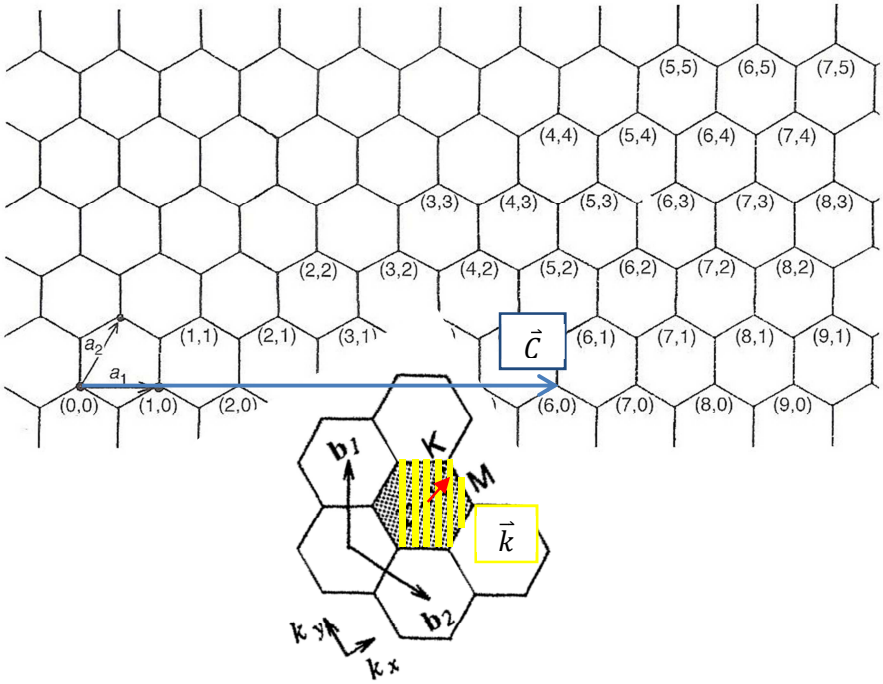

Figure 14: This figure illustrates the quantization of the wave vectors with a (6,0) zigzag tube. The chiral vector $\vec{C}$ is drawn in blue, and the corresponding allowed wave vector lines (branches) are drawn in yellow, while an example of allowed wave vector is drawn in red.

Another difference between the SWNT and the graphene sheet is that the density of states will present van Hoove singularities, infinite density of states for certain energies, because of the one dimensional character of the tube. So, while graphene is semiconductor with zero band gap, the Nanotubes with zero band gap will be metallic.

In conclusion, the chiralities, (n, m), for which the K point is crossed give metallic SWNTs, and the other chiralities correspond to semiconductor Nanotubes.

Equation (13) presents a relationship that gives directly which chiralities correspond to what type of tube.

$$\begin{cases} n - m = 3 \cdot q, & q\ integer \therefore metallic \\ n - m \neq 3 \cdot q, & q\ integer \therefore semiconductor \end{cases} \quad \text{Equation (13)}$$

From the above equation, it is readily seen that armchair SWNTs are always metallic.

The number of wave vector branches (Figure 14) increases with increasing SWNT diameter, because the distance between neighboring branches in inversely proportional to the chiral vector modulus, as one can infer from Equation (12). Reference [3] states that for diameters larger than $20\ nm$ there will be negligible gap. As a consequence, large diameter SWNTs and MWNTs (which have large diameters) are considered metallic.

2.4.1.2. Optical Properties

Optical techniques are widely used to characterize Carbon Nanotube structure, the main characterization techniques being: optical absorption, Photoluminescence, and Resonant Raman Spectroscopy. The first two will be presented in this section, and Raman Spectroscopy will be presented in a separate section due to its importance to Carbon Nanotube characterization, and because it is the technique used in this thesis.

The different optical characterization techniques depend on the possible optical transition energies ${E_{ii}}^{\alpha}$, where ii means that a photon is absorbed by an electron, which gets excited from the i^{th} branch (wave vector line) of the valence band to the corresponding i^{th} branch of the conduction band, and α is used to distinguish between semiconductor tubes and metallic tubes. An often used theoretical tool is the so called Kataura plot ([45]), which represents the transition energies ${E_{ii}}^{\alpha}$ for each SWNT.

In Figure 15, taken from [45], a Kataura plot represents transition energies, on the vertical axis, against tube diameters on the horizontal axis. Different chiralities present different transition energies, even for the same tube diameter. The vertical dispersion of the points on the plot (Figure 15) is due to the difference in chirality.

As can be seen from Figure 15, given a Nanotube sample with a certain diameter distribution, it might exist a laser excitation energy that would be absorbed exclusively by a group of metallic or semiconducting Nanotubes, or even more

PUC-Rio - Certificação Digital Nº 1011917/CB

specifically a determined chirality. This way, it is said that optical techniques have the potentiality to determine the Nanotube structure.

Furthermore, from Kataura plot (Figure 15) it can be seen that for lower laser energies the structural assignment becomes more unambiguous than for higher laser energies. Also, it can be observed that for smaller diameters the structural assignment becomes more unambiguous, than for larger diameters.

One of the above mentioned optical techniques is Optical Absorption, which serves to identify the presence of SWNTs in the sample, because MWNTs absorbs light in a continuum of energies. It can measure the ${E_{11}}^S$, ${E_{22}}^S$, and ${E_{11}}^M$, while higher transition energies overlap with σ orbital transition energies, and can not be identified ([7, p. 82]).

The drawback of Optical Absorption is its ambiguity, for many times, some chiralities have close transition optical energies, and can not be distinguished in the spectrum.

Photoluminescence (PL) is used to characterize semiconducting SWNTs only, because metallic tubes do not luminesce. In this technique a plot of emission energy versus absorbed energy is created. The absorbed photon energy is usually identified with ${E_{22}}^S$ while the emitted photon energy, with ${E_{11}}^S$, and the pair $({E_{22}}^S, {E_{11}}^S)$ can be used to determine the Nanotube's chirality, as in [46] and [47].

Figure 16 is an example of a PL plot from [46]. In the figure, excitation wavelength (the inverse of energy) is plotted against emission wavelength, and excitation is assigned to higher energies ${E_{ii}}^S$ $(i \geq 2)$, whereas emission is assigned to ${E_{11}}^S$.

PUC-Rio - Certificação Digital Nº 1011917/CB

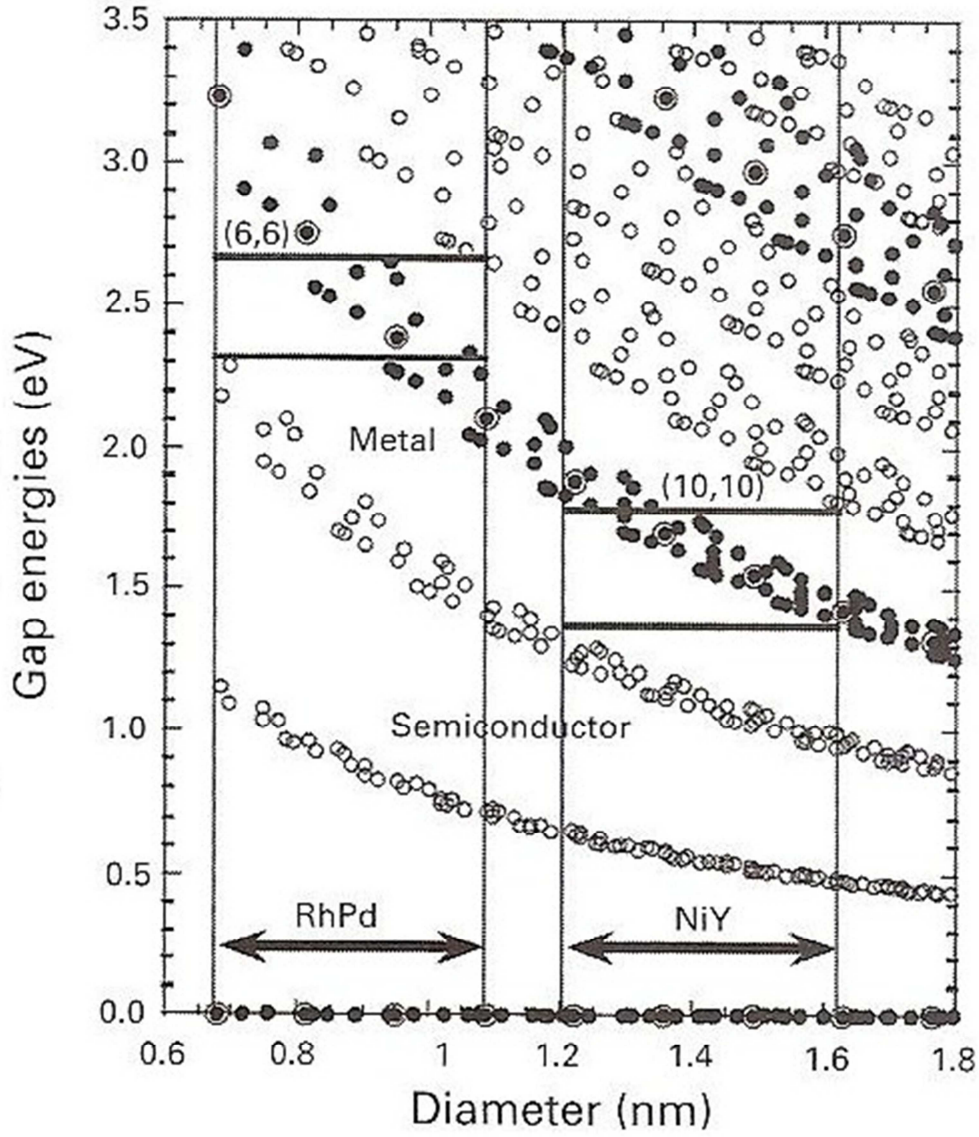

Figure 15: This Picture, taken from [45], is what is known as Kataura plot. The transition energies are plotted as a function of SWNT diameter, and the different types of dots represent different chirality tubes. The white ones are semiconductor tubes, the black ones are metallic tubes, and the double circle (whit black circle inside) are armchair tubes. The areas designated as RhPd and NiY represents the diameter ranges of the tubes produced with the respective catalysts in the work by Kataura [45]. The horizontal lines highlight the laser energy ranges that would only detect metallic SWNTs for each the samples

PL measurements have advantage in relation to Optical Absorption, because, by acquiring the additional information on the emission optical transition energy, it reduces the ambiguity in structure assignment.

In PL measurements, the Nanotubes must be isolated in order to luminesce. In [46] and [48], the authors disperse the SWNTs in a SDS/D_2O solution. In [47], the authors produce the Nanotubes over trenches in a Si/SiO_2 substrate, in a way that few crossed isolated from a trench to another, and could be measured.

PUC-Rio - Certificação Digital Nº 1011917/CB

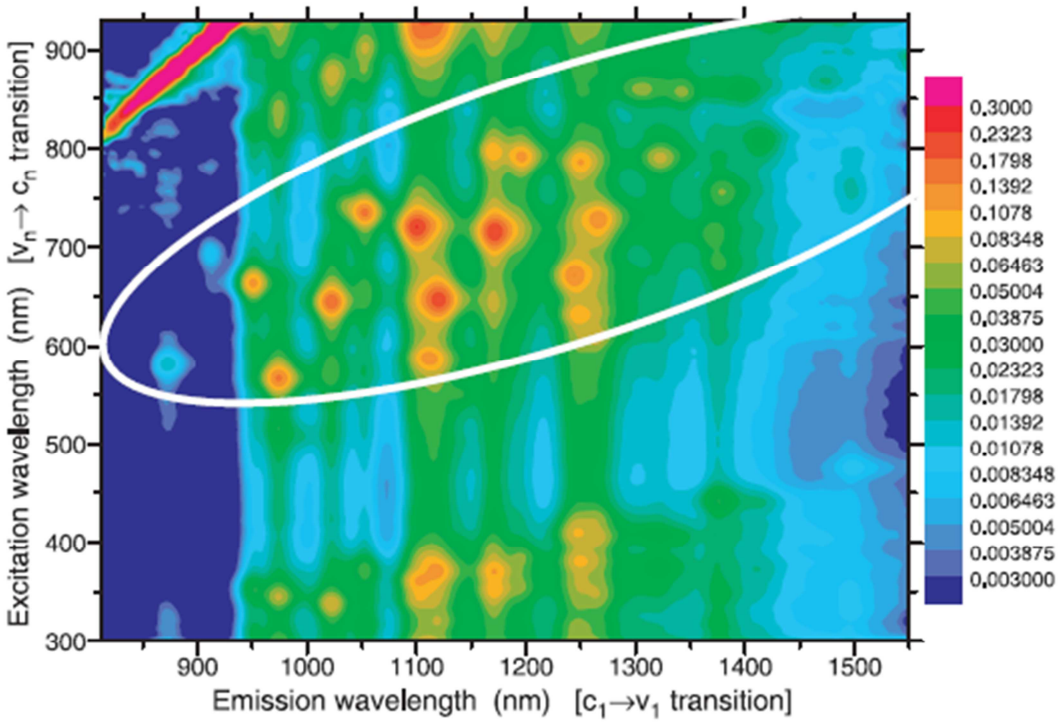

Figure 16: A PL plot taken from [46]: on the horizontal axis the measured emission wavelength which is assigned to ${E_{11}}^S$; on the vertical axis the measured excitation wavelength, assigned to higher transition energies ${E_{ii}}^S$, $i \geq 2$.

2.4.1.3. Raman Spectra of Carbon Nanotubes

While the other optical techniques were described in the last section, Raman Spectroscopy is analyzed separately in this section for its importance to this thesis.

As it was discussed in section " Raman Spectroscopy" (page 36), Raman intensity is maximized when there is a tuning between the incident photon energy and the intermediate state energy. It can be seen from Figure 15, that the optical transition energy depends on the Nanotube radius. Being this the intermediate state, one can reason that Raman intensity will be in resonance with the Nanotubes in a sample that match their optical transition energies with the laser energy, [49].

Raman Spectroscopy gives more information than the Optical Absorption technique because, besides the information on the energy gap between valence and conduction band, it gives a full spectrum, with peculiar peaks, that might give further information on the Nanotube structure. Furthermore, it can be used to characterize also MWNTs.

It has been said in section " Raman Spectroscopy" that Raman technique can be used to probe a molecule's vibrational and rotational states. In the case of Carbon Nanotubes, it must be noted that not a finite, but an infinite number of vibrational modes are present because of the practically infinite size of the molecule in relation to the interatomic distance. The infinite vibrational modes are identified with mechanical waves along the Nanotube structure: the Phonons. Each Phonon is a normal mode of vibration of the Carbon Nanotube lattice, and its interaction

PUC-Rio - Certificação Digital Nº 1011917/CB

with the electrons happens when the phonon respects some symmetry conditions imposed by quantum mechanical selection-rules.

The main peaks, or modes, studied in Raman Spectroscopy of Carbon Nanotubes are Radial Breathing Mode (RBM), Tangential Mode (G), Disorder Induced Mode (D), and Second Order Tangential Mode (G'). They will be discussed in the following paragraphs.

There are many good reviews on the topic of Raman characterization of Nanotubes, of which it may be mentioned [39], [50], [51], and [7, p. 251 - 286].

2.4.1.3.1. Radial Breathing Mode (RBM)

This Raman mode corresponds to uniform stretching and squeezing of $C-C$ bonds, resulting in a radial movement of the tube, which resembles a breathing movement. It is observed at Raman shifts around $100\ cm^{-1}$ to $300\ cm^{-1}$.

The most important characteristic of the RBM is its dependency to Nanotube diameter, as can be seen in, for example in [45], [46], and [52]. The relationship between Raman shift and tube diameter is of the functional type:

$$\omega_{RBM} = \frac{A}{d} + B \qquad \text{Equation (14)}$$

The coefficients A and B will depend on ambient conditions, such as temperature, pressure, chemical environment, doping, Nanotube bundling, etc. But for isolated Nanotubes [46] used the values $A = 223.5 cm^{-1}.nm$ and $B = 12.5 cm^{-1}$, [52] used $A = 248 cm^{-1}.nm$ and $B = 0 cm^{-1}$, and [53] $A = 217.8 cm^{-1}.nm$ and $B = 15.7 cm^{-1}$. Figure 17, taken [53], illustrates Equation (14), by fitting experimental points with parameters $A = 217.8 cm^{-1}.nm$ and $B = 15.7 cm^{-1}$.

For an individual SWNT, the RBM band width increases with increasing diameter, as well as the Raman cross section decreases with diameter, [7]. This way MWNTs and large diameter SWNTs will not present the RBM mode, which is used as an evidence for the presence of SWNTs in a sample.

Like Optical Absorption, and PL techniques, RBM Raman mode can be used to determine SWNTs chirality, as in [54], and [52]. By exciting a sample with different laser energies, and measuring the position and intensity of the RBM mode, and 2 dimensional plot can be made of photon energy, E_{ph}, against RBM Resonant Raman shift, ω_{RBM}, which can be identified as a $(E_{ii}\ , d)$ plot. This plot can be directly compared to Kataura plot to determine the structure (n, m) of the Nanotube. This methodology is used in paper [52] to characterize isolated SWNTs on a Si/SiO_2 substrate, as can be seen in Table 1.

PUC-Rio - Certificação Digital Nº 1011917/CB

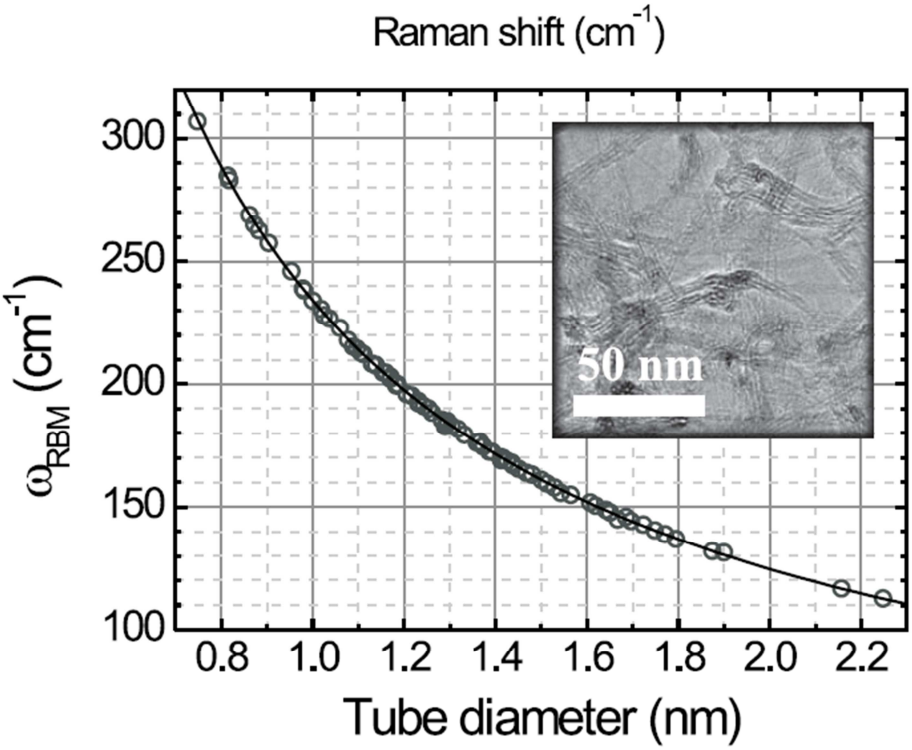

Figure 17: This figure, taken from [53], shows experimental points fitted with the parameters $A = 217.8cm^{-1}.nm$ and $B = 15.7cm^{-1}$.

TABLE II. Possible chiralities predicted for semiconducting nanotubes and their ω_{RBM} (calculated and observed) in the resonant window $1.48 < E_{22}^{S} < 1.68$ eV.

(n,m)	d_t [nm]	θ [deg]	ω_{RBM} [cm^{-1}] (calc.)	(expt.)	E_{22}^{S} [a] [eV]
(14, 1)	1.15	3.4	215.1	210(1)	1.50
(10, 6)	1.11	21.8	223.1	···	1.51
(9, 7)	1.10	25.9	224.9	···	1.48
(11, 4)	1.07	14.9	232.2	229(1)	**1.60**
(10, 5)	1.05	19.1	236.1	237(2)	**1.54**
(12, 2)	1.04	7.6	238.2	···	1.66
(8, 7)	1.03	27.8	240.3	239(2)	**1.61**
(11, 3)	1.01	11.7	244.7	···	**1.57**

[a]Bold face indicates a strong resonance.

Table 1: This table, from [52] illustrates how one can assign chirality of an individual SWNT by knowing the RBM peak position, given a specific laser energy. After assignment, the author calculated the theoretical RBM position ("calc." column) and compared with the experimental value ("expt." column).

PUC-Rio - Certificação Digital Nº 1011917/CB

Qualitatively, in [53] a Kataura like plot is built based on the measurement of Raman intensities in the RBM range of frequencies, with different laser energies. By comparing their experimental plot with theoretical Kataura plot, the authors are able to identify each optical transition branch, and the metallic/semiconducting character of the tubes (Figure 18).

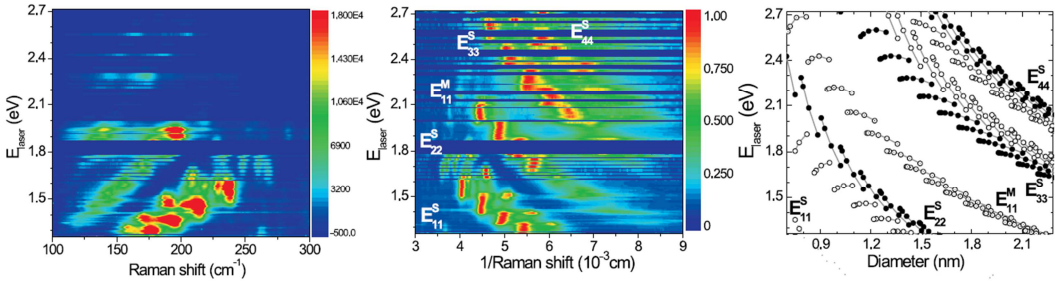

Figure 18: This figure shows the construction of a Kataura like plot from reference [53]. On the left panel, the laser energies versus the measured Raman shifts. On the central panel, the horizontal axis is substituted by the inverse of Raman shift, for it should be proportional to diameter. On the right panel the theoretical Kataura plot. By comparing the right panel with the central one, the authors managed to identify each optical transition branch and the metallic/semiconductor character.

2.4.1.3.2. Tangential Mode (G)

Carbon Nanotube's G band is inherited from graphite. It corresponds to in plane (tangential) movements of Carbon atoms. Whereas on graphite G mode is a peak centered at 1582cm^{-1}, in SWNTs this doubly degenerate mode split into two modes, G^+ and G^-, because of the symmetry break imposed by the curvature of along the chiral vector direction. The resulting modes are called circumferential (TO), and axial (LO) modes.

The frequency distance between G^+ and G^- is dependent on Nanotube diameter, thus can be used to confirm information from RBM mode, and the presence of G^- and G^+ separation is a evidence of the presence of single-wall in a sample.

These modes present usually a Lorentzian lineshape, in agreement to Equation (8).

These modes of vibration also bear relationship with the metallic or semiconductor character: in semiconducting SWNTs, G^- corresponds to TO mode and G^+ corresponds to LO mode; in metallic SWNTs, G^- corresponds to LO and G^+ corresponds to TO, and their corresponding peak distance is bigger. Another difference is that, in metallic SWNTs, G^- is described by Breit-Wigner-Fano lineshape, not Lorentzian.

A detailed study on G band modes is accomplished in the reference [55] using laser wavelength $514.5\,nm$. In this paper, the authors do Raman spectroscopy on individual SWNTs. They assign chirality to each Nanotube based on the RBM position and laser energy (Kataura plot approach), and use this information to understand the dependency of G^+ and G^- peaks on diameter, chirality and metallic/semiconductor character. First, it is concluded that the separation between the peaks depends only on diameter and on the metallic/semiconductor character, by the following relationship:

PUC-Rio - Certificação Digital Nº 1011917/CB

$$\omega_{G^+} - \omega_{G^-} = {}^{C}/_{d^2} \qquad \text{Equation (15)}$$

Where, C equals to $47.7cm^{-1}.nm^2$ for semiconductor tubes, and $79.5cm^{-1}.nm^2$ for metallic tubes. The G^+ position ω_{G^+} is found, by the authors, to be independent on diameter or metallic/semiconductor character, and equals to $1591cm^{-1}$. These relations are illustrated in Figure 19, adapted from the same paper [55].

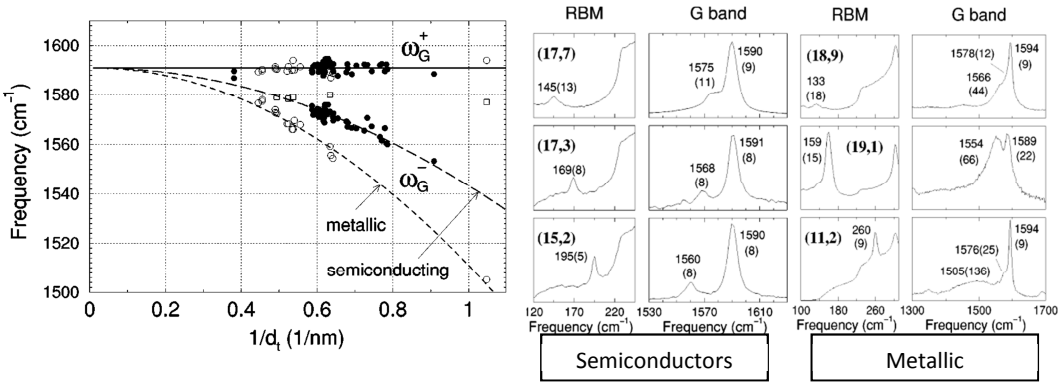

Figure 19: This figure, adapted from different figures of reference [55], illustrates the effect of SWNT diameter on G^+ and G^- separation. On the left panel, experimental measurements of the peak positions. The black circles represent the peak positions of the semiconducting tubes, while the white ones, the metallic tubes. The upper circles are the G^+ peak position, represented by $\omega_{G}{}^{+}$, and they are fitted by a constant line at $1591cm^{-1}$, while the bottom ones are the G^- peaks, represented by $\omega_{G}{}^{-}$, and are fitted by two different curves: one for the metallic tubes, the other for the semiconducting ones. On the center and right panels, the actual Raman spectra from which data was taken to make the plot on the left. It can be noted that as the RBM mode shifts to higher frequencies, the G^- peak shifts to lower frequencies, and the G^+ does not move. It can also be noted the difference in G^- lineshape between semiconducting (Lorentzian) and metallic (BWF) SWNTs. The peaks positions and bandwidths (in parenthesis) are in cm^{-1} units

It can also be noticed, in Figure 19, the difference in line shape between G^- peak for semiconducting (symmetric Lorentzians) in comparison to metallic tubes (asymmetric Breit-Wigner-Fano, or BWF).

The G band is influenced by doping, as will be discussed in the next section (" Raman Spectrum of doped Nanotubes").

2.4.1.3.3. Disorder Induced Band (D)

The D band is also inherited from graphite, and appears between $1300\ cm^{-1}$ to $1400\ cm^{-1}$. It originates from symmetry break of SWNTs periodic structure by defects, such as Stone-Wales defects, doping, missing Carbon atoms in the Nanotube lattice, tube termination, etc.

The D mode comes from a second-order Raman process. It means that the excited electron is scattered in two steps before emitting scattered light, instead of just one, as happens in first-order Raman processes. In the case of D band, the electron is scattered by a phonon, and a defect, [7, p. 260].

PUC-Rio - Certificação Digital Nº 1011917/CB

The most common way of characterizing D band is by measuring the intensity (or area) ratio between D and G band, that is I_D/I_G (or A_D/A_G), where the D mode is fitted usually by a Lorentzian line shape. The higher the ratio, the more defective is considered the Nanotube.

2.4.1.3.4. G' Band

G' band is another second order Raman process inherited from graphite, in which the excited electron is scattered by two phonons before emitting a photon. Its frequency position is twice the frequency of the D band, [7, p. 261].

G' band in SWNTs might be composed of more than one peak, and these two peaks splitting depend on the electronic structure of the Nanotube, [56]. As will be discussed in the following section, this G' band splitting is influenced by doping.

2.4.2. Physical properties of Boron doped Carbon Nanotubes

In this section, the above mentioned physical properties of pristine Carbon Nanotubes will be compared to Boron doped Carbon Nanotubes, in special SWNTs, so that the experimental results of this thesis can be better understood and interpreted.

2.4.2.1. Electronic Properties

To understand the electronic properties of B doped Carbon Nanotubes, one can start out from understanding pristine Carbon Nanotube electronic properties, and check for the changes that happen when adding Boron atoms.

From a rigid band model, used in solid state Physics to study doping of silicon for example, adding Boron atoms to the Carbon Nanotube lattice, at low concentrations should not change the established electronic band structure of the pristine material, but create an acceptor or donor dispersion less level in between the valence and conduction bands.

Given prior knowledge from Boron doped sp^2 Carbon systems, such as graphite, it can be expected that Boron will act like an electron acceptor in Carbon Nanotubes, creating an acceptor level under the Fermi level, that is, close to the valence band. This level will accept electrons from the valence band, and will donate holes to the valence band, to be charge carriers. For this reason, Boron doping of sp^2 Carbon systems is said to be p-type, in contrast to n-type doping, when electrons are donated by the heteroatom to the conduction band, to be charge carriers.

As the B concentration rises the new acceptor level wavefunctions start to get more and more delocalized, and the initial acceptor level will present energy dispersion character. Plus, the pristine Carbon Nanotube original bands will start to be modified.

PUC-Rio - Certificação Digital Nº 1011917/CB

It has been originally calculated, [57], that for low concentrations B doping will create an acceptor level 0.16eV above the valence band. The authors use zigzag semiconductor (8,0) and 1.25% doping.

In relation to MWNTs it is has been experimentally shown that B doped tubes present intrinsic metallic behavior, as measured in [16,18,11], and an enhanced conductivity, in comparison to undoped MWNTs.

However, it is agreed that Boron doping will lower the Fermi level, thus lowering the highest occupied energy in the valence band. This will increase the energy gap for optical transition, and will, then influence optical and Raman properties, as will be discussed in the following sections.

2.4.2.2. Optical properties

In brief, optical properties of Boron doped Carbon Nanotubes will change because of the lowering of the Fermi level. For example, in highly doped semiconductor SWNTs, $E_{11}{}^{S}$ transition will not be possible, because the first branch of the valence band will be depleted, as shown by theoretical calculations and optical absorption spectra in [58], and [59].

Figure 20 is adapted from [58]. It illustrates the above mentioned effect. The Optical Absorption Spectrum shows an inhibition of the $E_{11}{}^{S}$ and $E_{22}{}^{S}$ optical transitions for Boron doped SWNTs. This behavior can be explained by the depletion of the corresponding bands, as can be seen from the density of states plots.

On the other hand, Figure 20 shows a peak around 0.4eV which appears for the doped Nanotubes. The authors explain it in terms of excitation of valence electrons into the acceptor band created by Boron.

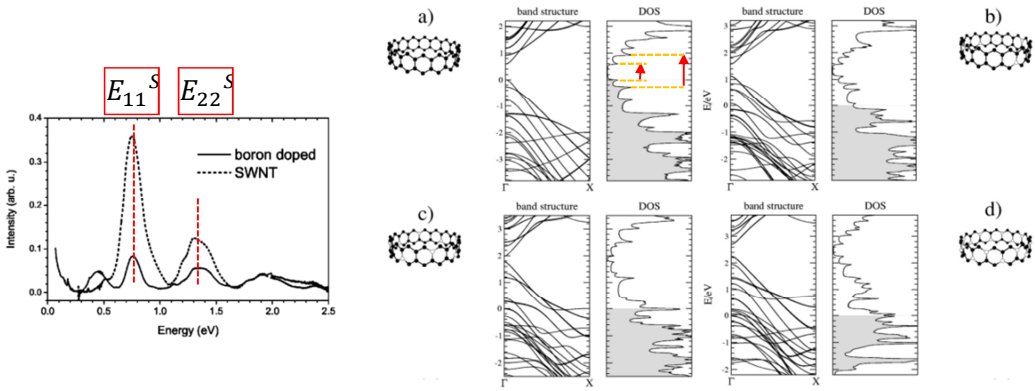

Figure 20: This figure, adapted from [58], shows the effect of Boron doping on the Optical Absorption Spectra. The two peaks assigned on the left side as $E_{11}{}^{S}$, and $E_{22}{}^{S}$ correspond on the right panel to the smaller arrow and longer arrow transitions, respectively. On the right side, there are representations of energy dispersion relations (band structure), density of states (DOS), and the insets are a geometric representation of a unit cell of the SWNT, with Carbon atoms plotted as black circles, and Boron atoms plotted as white circles. The shaded areas in the DOS panels represent occupied electronic states. From (a) to (d) it is represented 0%, 6.25%, 12.5%, and 25% doping.

PUC-Rio - Certificação Digital Nº 1011917/CB

Even at low concentrations, the effect of Boron doping will be to upshift in energy and decrease in intensity the original optical transition peaks. This will have consequences for the Raman spectra of Boron doped SWNTs.

2.4.2.3. Raman Spectrum of doped Nanotubes

According to [7], the main changes in Raman spectra due to doping (p or n type) are shifts of the G and G′ peak positions, changes in peak amplitudes (for example, $^{I_D}/_{I_G}$ ratio), broadening or narrowing of bandwidths, creation of new peaks (such as D′), and deformation of peaks (such as G′, as will be seen in the next paragraphs).

In the case of Boron doped SWNTs, a general upshift in the spectra should be expected from the electronic point of view, for the depletion of the valence bands due to electron transfer from the valence band of the tubes, to the acceptor level of Boron. As discussed in the previous section, this charge transfer will increase the energy gap between the highest occupied energy in the valence band and the conduction band. On the other hand, Raman Spectrum depends on the phonon energy dispersion relations too, and as B concentration is increased a weakening is expected for the Carbon Nanotube lattice, as $B-C$ bond is weaker than $C-C$ bond (Bond Dissociation Energies 444 and 600 kJ/mol, respectively [60]). The literature findings on the topic of Raman characterization of Boron doped Carbon Nanotubes are presented below.

Reference [54], asserts that a general upshift is expected to happen for p-type doping, because of electron transfer from the Carbon valence band to the acceptor level of the dopant. In this reference, exohedral doping with either I_2 and Br_2 (acceptors) is compared with exohedral doping with either K and Rb (donors).

In the case of Boron doping, which is also p-type, [61] measures upshifts of the G^+mode up to 4 cm^{-1} for doping levels around 1%. Upshifts of 5 to 9 cm^{-1} in the G^- peak are reported, but there is no evidence that this is a doping effect, and not a diameter dependent effect (as shown in last section). G^- intensity is reported to become smaller.

The $^{I_D}/_{I_G}$ ratio is expected to increase with respect to Boron concentration if one considers B atoms as point defects in the Carbon lattice. In [14], an increase in the ratio for increasing Boron concentration is observed, and related to a decrease of graphitization, and crystallinity. But reference [61] describes negligible change in this respect.

In [32], G^+ band is upshifted at the same time that separation of G^+ and G^- peaks decreases to zero, and $^{I_D}/_{I_G}$ increases.

In reference [37], a study of Raman features of Boron doped Carbon Nanotubes. Although the focus in this paper is DWNTs, some of the observed behaviors may fit within this section. The D and G bands upshift in frequency by 7 cm^{-1} and 5 cm^{-1}, respectively, as measured doping increases from 0% (pristine) to 3%.

PUC-Rio - Certificação Digital Nº 1011917/CB

I_D/I_G ratio, and D band bandwidth increase, and are related by the authors to the presence of Boron within the Nanotube lattice. G' band is downshifted 7 cm^{-1} and its intensity decreases, as a result of $B-C$ bond being weaker than $C-C$ bond, as argued by the authors.

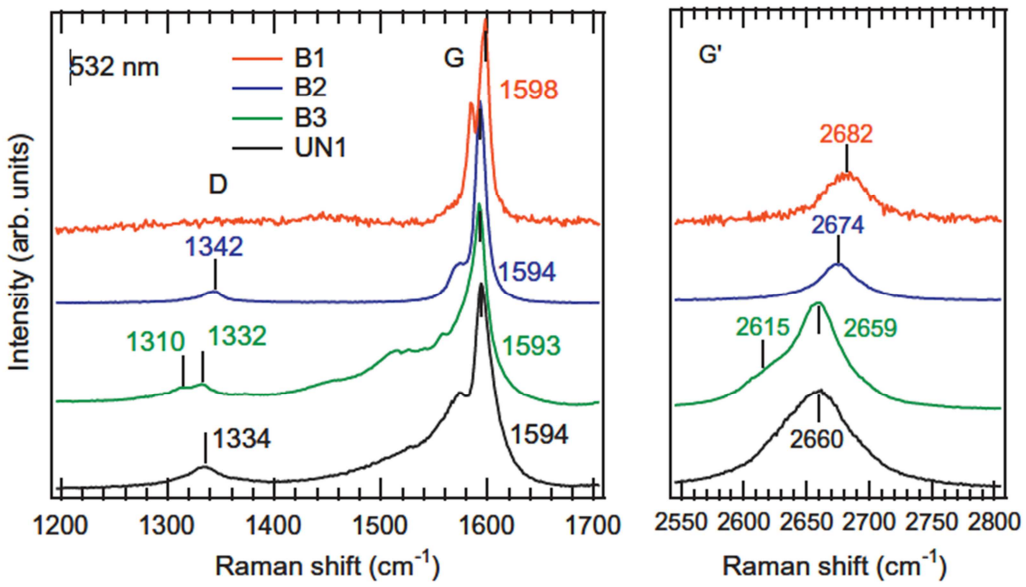

Figure 21: This figure was taken from [61], and illustrated the G^+ peak shift, when doping levels increase (left panel). Also, on the right panel, upshift on the peak position, is reported.

In summary, the results found in the literature are not always consistent with one another. On the other hand, it can be understood that Raman, is a powerful tool for characterizing Boron doped Carbon Nanotubes, because even at low concentrations, the majority of the results in the literature report noticeable changes in Raman spectra, while the rest of the characterization techniques fail detect any change.

2.5. Methods for doping characterization

To characterize the amount of doping, and to probe its physical effects on the Carbon Nanotube, or even just to indirectly evidence existence of doping, some characterization techniques beyond the above mentioned ones are found in literature. As a final section in this review of the state of the art in Boron doped Carbon Nanotube systems, a summary is presented as to the main methods of doping characterization found in literature.

Spectral chemical analysis, such as electron energy loss spectroscopy (EELS) [18,31,32,58] and XPS [15,34,35,37,61], are used to evidence the existence of Boron on the sample, and its direct bonding to Carbon atoms. At high enough concentrations, around 1%, they can estimate the amount of doping ([32] for example fail to measure low doping level with EELS), although still no standard

PUC-Rio - Certificação Digital Nº 1011917/CB

has been settled as to quantitative analysis of doping levels SWNTs, because curvature effects on the $B1s$ spectra is still a matter under discussion [35].

Optical Absorption has been used as an evidence for the electronic effect that B has on the Nanotube [58,59].

Raman analysis is the main tool for characterizing the physical properties of Boron doped Carbon Nanotubes in comparison to pristine tubes, and it is used both in the case of SWNTs, [15,35,61,62], DWNTs [37] and MWNTs [18], [14]. Raman spectrum is sensitive to doping levels undetectable by EELS and XPS, and this makes this technique a powerful tool to characterize doped Carbon Nanotubes.

X-Ray Diffraction (XRD) is used to detect structural consequences of Boron on the Nanotubes. In [17], [18] and [63], it is used to detect the degree of crystallinity of doped MWNTs. In [37], XRD is used to demonstrate an increase in interlayer spacing (in contrast to [63]), and increased disorder; the authors argue that in situ doping methods, like CVD will result in decreased crystallinity, while substitution reactions will result in increased crystallinity of Boron doped SWNTs.

Like X-Ray diffraction, electron diffraction is used to probe Carbon Nanotube structure. It is used in [17] and [18] to assign helicity (chirality) to individual Boron doped MWNTs, and identify helical alignment between tube walls.

Scanning electron microscopy (SEM), and transmission electron microscopy (TEM) are also used to probe the structural changes of Boron doped Carbon Nanotubes. For example, High resolution TEM (HRTEM) can measure interlayer spacing in individual MWNTs, and as well as assign chirality. SEM images are used to characterize production yield, Nanotube length, and can be used as indirect evidence to defect levels in Nanotubes, by observing Nanotubes morphology. SEM and TEM images are present in many of the references.

Electric measurements are used to directly probe the electronic properties of doped systems. In [32], Thermopower measurements are used to prove intrinsic p-type doping, and thus evidence doping, at concentrations undetectable by EELS. [16], and [18] use microwave conductance measurements to prove intrinsic metallic behavior of B doped MWNTS. Field emission measurements are also used [12], [14], to show improved emission properties of Boron doped Carbon Nanotubes over pristine ones.

Scanning Tunneling Spectroscopy has been used to characterize electronic properties of doped tubes by [11].

PUC-Rio - Certificação Digital Nº 1011917/CB